TOWARDS REALIZING THE LOW-COERCIVE FIELD OPERATION OF SPUTTERED FERROELECTRIC $Sc_xAl_{1-x}N$

Ved Gund[1], Benyamin Davaji[1], Hyunjea Lee[2], Joseph Casamento[2], Huili Grace Xing[2], Debdeep Jena[2], and Amit Lal[1]

[1]SonicMEMS Laboratory, Cornell University, NY, USA

[2]Jena-Xing Laboratory, Cornell University, NY, USA

2021 21st International Conference on Solid-State Sensors, Actuators and Microsystems (Transducers) | 978-1-6654-1267-4/21/$31.00 ©2021 IEEE | DOI: 10.1109/TRANSDUCERS50396.2021.9495515

ABSTRACT

In this paper, we map the ferroelectric properties of 22% and 30% scandium-doped aluminum nitride (ScAlN) thin films with the goal to engineer low coercive fields for low-voltage post-CMOS compatible RF frontends. ScAlN films, 200 nm and 300 nm thick, were deposited on platinum and molybdenum electrodes. Lateral and vertical capacitors were tested across various electric field strengths, frequencies, and electrode sizes. Measured coercive field and remnant polarization values were between 3.9-6.2 MV/cm and 58-170 μC/cm^2. Frequency and device area-dependence were studied to identify trends towards low coercive fields. A comparison of lateral and vertical capacitors on the same ScAlN films shows the impact of charge-traps due to current-crowding in lateral devices. Finally, an anomalous observation relating doping concentration and film stress with coercive field and remnant polarization is reported to present the potential for decoupled tuning knobs for ferroelectric engineering properties ScAlN.

KEYWORDS

Ferroelectrics, ScAlN, Coercive field, Leakage current

INTRODUCTION

Aluminum nitride (AlN) is the material of choice for MEMS RF resonators due to its excellent piezoelectric properties, high-quality factor, and CMOS compatible sputter deposition and processing [1], [2]. Fundamental limits in the piezoelectric properties of AlN has inspired the exploration of new materials with enhanced properties. Scandium-doped AlN (ScAlN) has generated significant interest for this purpose because of the similarity in processing to AlN, while presenting a tuning mechanism to increase the piezoelectric coefficient 4x larger by changing the Sc-doping [3]. Furthermore, AlN has a non-centrosymmetric wurtzite structure with spontaneous polarization but has not been shown to be ferroelectric because the switching field exceeds the dielectric breakdown field [4]. Ab initio calculations predict that monotonically increasing Sc-doping of AlN can soften the ionic potential energy landscape and decrease the barrier necessary to transition between the parent wurtzite structure and the hexagonal phase in ScAlN, thus producing ferroelectric switching in ScAlN [5].

The recent discovery of ferroelectric switching in highly doped ScAlN, with Sc-doping >27%, has confirmed theoretical predictions and generated significant interest as the first III-V ferroelectric material [6]. Following this, the impact of gas flows on crystal growth, stress, and surface roughness has been optimized for 29% ScAlN films [7]. Ferroelectricity in 30% ScAlN has been utilized for frequency tuning and bandwidth reconfigurability of GHz acoustic filters geared towards 5G standards [8], [9]. Ferroelectric switching has also been demonstrated with Sc-doping as low as 10% but the required switching fields (> 7 MV/cm) can approach the the dielectric breakdown [10]. Efforts to characterize the piezoelectric and dielectric properties of ferroelectric materials have identified high leakage currents and larger coercive fields in ScAlN as a key challenge in the integration of these films in RF devices [11]. This paper presents experimental results of testing 22% and 30% doped ScAlN capacitors to map out the space of coercive fields (E_C) and remnant polarization (P_r) across a range of electrode sizes and operation frequencies. Additionally, the impact of underlying electrodes and observations of the impact of film stress on the films' ferroelectric properties is investigated. The data provides a pathway to accelerate the engineering of lower E_C in ScAlN.

Table 1: Summary of 4 different film stacks tested for measuring ferroelectric properties of 22% and 30% ScAlN

	Substrate	Film Stack	σ in MPa	XRD-FWHM
A	SiO_2/Si	AlN seed/Mo BE/AlN seed/ 300 nm $Sc_{0.3}Al_{0.7}N$/Al TE	-192	2.4^0
B	SiO_2/Si	AlN seed/Mo BE/AlN seed/ 200 nm $Sc_{0.3}Al_{0.7}N$/Mo TE	-86	3.6^0
C	Si	Pt/200 nm $Sc_{0.3}Al_{0.7}N$/Mo	-83	3.1^0
D	SiO_2/Si	Pt/200 nm $Sc_{0.22}Al_{0.78}N$/Mo	102	3.0^0

DEVICE FABRICATION

Table 1 summarizes the list of ScAlN film stacks tested. ScAlN films with 22% and 30% Sc-doping and thicknesses of 200 and 300 nm were deposited by reactive co-sputtering using an OEM Endeavor PVD cluster tool that has a dual-target S-gun magnetron [12]. For all depositions, 200 nm sputter-deposited metal films were used to realize the continuous bottom electrode (BE) and patterned top electrode (TE). A 30 nm AlN seed layer was deposited on top of the BE to texture the ScAlN deposition. For samples A and B, the film stack was deposited on 1 μm SiO_2 grown on high-resistance (100) silicon. Next, a 30 nm AlN seed layer was deposited to template the molybdenum (Mo) BE, and 30%-doped ScAlN films of 200 nm and 300 nm were deposited without an air-break. Mo and Al TE were then sputtered on the 200 and 300 nm ScAlN films, respectively, and patterned with subtractive etching to

realize the final capacitors. For samples C and D, platinum (Pt) BE films were sputter-deposited to template a 30 nm AlN seed for 22% and 30% 200 nm ScAlN films, followed by in situ Mo TE deposition. All 200 nm ScAlN films were subsequently patterned and plasma-etched using chlorine-based chemistry [13] to enable both TE and BE access for electrical probing. The film stress σ and Full Width Half Maximum (FWHM) of the XRD Rocking Curve (RC) for the films were also measured after deposition.

TEST SETUP

Figure 1A shows the Sawyer-Tower circuit assembled to test the ferroelectric capacitors with a custom probe station [14]. The films were tested with continuous wave positive-up-negative-down (PUND) input waveforms and triangular pulses of equal rise, fall, and wait times [15]. A Rigol DG1022 Arbitrary Waveform Generator was used to program the input signal, which was amplified with a Piezo Systems EPA-102 amplifier with 400V peak-to-peak output and 250 kHz bandwidth. This system enabled high E-fields up to 10 MV/cm and 6.6 MV/cm in the 200 nm and 300 nm ScAlN respectively. A series resistor $R_{sense} = 11.6\ k\Omega$ was used to measure the switching currents with the resistor value chosen to have a minimal impact on the voltage divider with the drive capacitor.

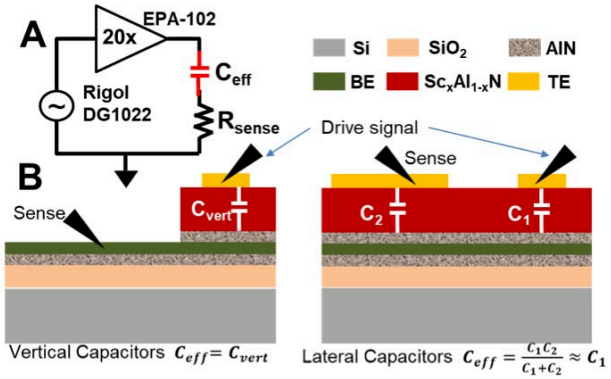

Figure 1: A). Modified Sawyer-Tower circuit for testing ferroelectric ScAlN capacitors. B). Probing configurations for testing vertical and lateral capacitors.

Figure 1B shows the two different test structures used for measurements reported here. Vertical capacitors with the drive signal applied to the TE and sense-current measured from the BE were tested, in devices where BE access was possible for 200 nm ScAlN film. For the 300 nm ScAlN with only TE access, a large capacitor (30-800x larger than drive capacitance) was used for the sense current probe such that the series combination with the drive capacitor, utilizing an intermediate floating BE is approximately equal to the drive capacitance. To map the devices' ferroelectric properties, ScAlN capacitors with circular electrodes ranging in diameter from 20-100 µm were tested for ferroelectricity between 1.5-7.5 kHz.

EXPERIMENTAL RESULTS

Representative data from sample A (300 nm $Sc_{0.3}Al_{0..7}N$ on Mo BE) with 50 µm diameter shows the testing methodology used (Figure 2). The raw voltage on R_{sense} shows clear peaks in the switching and leakage currents in the range of 1.5-7.5 kHz (Fig. 2A) with a PUND input waveform shown in the inset. To remove the non-switching and leakage components, the U and D components were subtracted from the P and N to plot just the switching current density vs input E-field (Fig. 2B). A clear peak was observed in the current density at the corresponding E_C for each frequency. The current data was integrated to realize the P-E loops (Fig. 2C) and extract E_C and P_r for the tested devices. Depending on the Sc-doping, film thickness, underlying BE, and film stress, E_C and P_r were measured in the range of 3.9-6.2 MV/cm and 58-170 µC/cm^2 respectively.

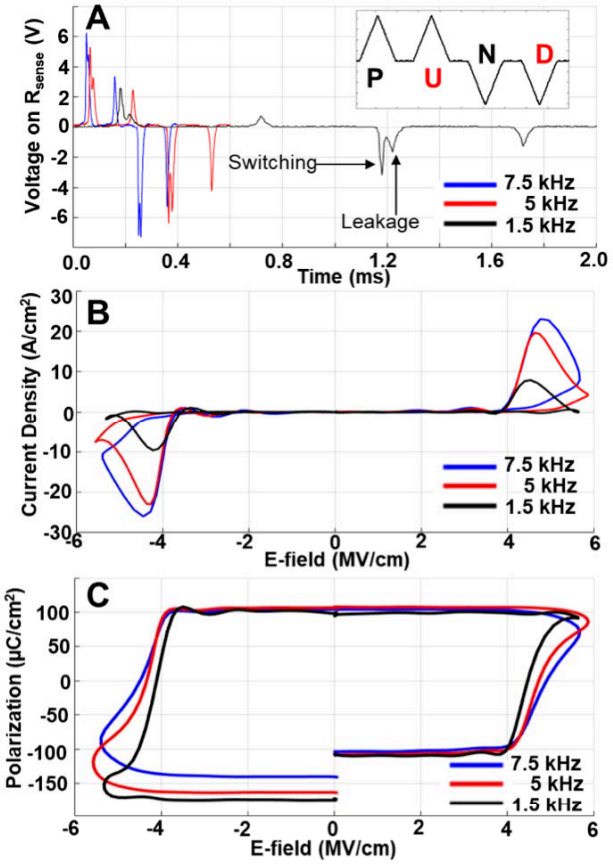

Figure 2: A). Raw voltage waveforms on R_{sense} at various switching frequencies for PUND test (generic input waveform in inset). B). P-U and N-D switching current density vs. E-field showing peaks in the current at the corresponding E_C for each frequency. C). Polarization vs. E-field (PE) loops generated by integrating switching currents from B to extract E_C and P_r.

Frequency & Area-Dependence of Ferroelectricity

High leakage currents and large Ec values, close to the dielectric breakdown E_{BD}, are a significant challenge for reliable ferroelectric switching in ScAlN [6], [7]. Our experiments confirm that the observed breakdown (E_{BD} ~ 7 MV/cm) is filamentary, which produces a short circuit through the ferroelectric film, and is not thermally generated due to high switching power, which would instead lead to catastrophic ablation of the electrodes. As such, the area of the capacitors and frequency of PUND switching play a key role in setting the E_C and P_r for ScAlN. Figure 3 plots E_C and P_r vs. switching frequency for capacitors ranging in diameter from 20-100 µm for samples

B (200 nm 30% ScAlN on Mo) and D (200 nm 22% ScAlN on Pt). Frequency-dependence: In both samples, E_C increases and P_r decreases with an increase in frequency. The increase in E_C can be explained by a thermally activated process for the switching resistance and demonstrates a weak frequency-dependence similar to other ferroelectrics such as PZT [16]. The reduced P_r is a likely consequence of incomplete switching leading to lower polarization charge at higher frequencies. For lower switching frequencies approaching 1.5 kHz, E_C converges to 5.45 MV/cm and 5.2 MV/cm over the range of capacitor sizes tested in samples B and D respectively. The convergence indicates that the switching occurs sufficiently slowly to approach area-independence and close to the actual E_C for ScAlN. Area-dependence: For a fixed switching frequency, E_C decreases as capacitor size increases, whereas P_r increases. We hypothesize that larger electrodes reduce the barrier for switching (and leakage) since they are likely to encompass multiple parallel pathways for switching due to a larger number of grains, thus enabling ferroelectric transition at fields as low as 5.1 MV/cm in this case.

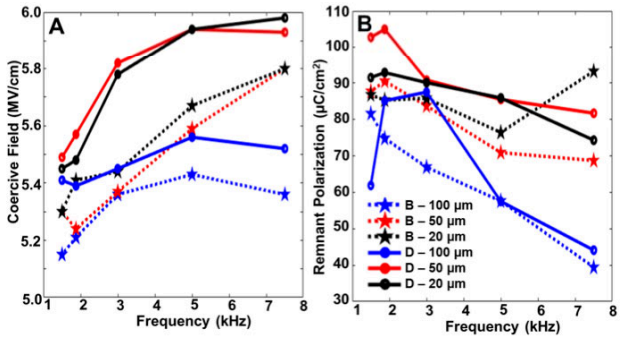

Figure 3: Plots of A). E_C and B). P_r vs. frequency for capacitors of 20-100 μm diameter with 30% and 22% doped ScAlN on Mo and Pt electrodes (samples B and D) to map frequency and area-dependence of ferroelectricity.

Vertical vs. Lateral Capacitors

Here, lateral capacitors with a large metal pad as a sense electrode were compared with vertical devices that have BE access. It has been previously reported that lateral devices are better suited to reduce the leakage current since there are two AlN barrier layers in the signal path compared to just one layer for the vertical devices [11]. For identical drive electrode sizes, these two configurations have nearly equal capacitances, so any differences in ferroelectric properties arises from the physical device structure and AlN barrier layers. Figure 4 shows the current density vs. E-field and PE loops for 22% ScAlN 200 nm thin film capacitors with 50 μm diameter on Pt on the same die. The vertical device (blue trace) has equal non-switching current contributions in the P/U and N/D pulses, leading to a single peak in the current density vs E-field plot. However, the lateral devices suffer from unequal non-switching currents, likely due to the presence of charge traps as a result of current-crowding, leading to a second peak in the switching current [17]. Consequently, the E_C appears to favorably decrease from 5.8 MV/cm to 5.34 MV/cm and P_r appears to increase 91.5 μC/cm^2 to 140 μC/cm^2. To mitigate the effect of traps in lateral capacitors, measurements can be performed at elevated temperature or higher frequencies, allowing trapped charges to dissipate rapidly while still harnessing the reduced leakage current due to two AlN barrier layers in the signal path.

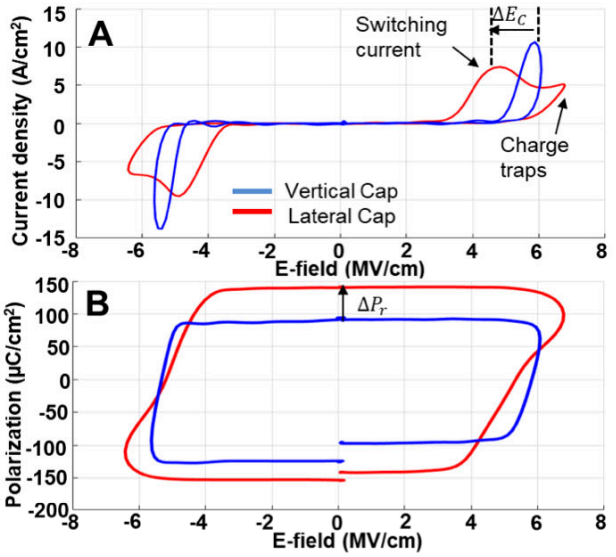

Figure 4. A). Current density vs E-field for lateral and vertical capacitors on 200 nm 22% ScAlN. Dual peaks in the current density show the contribution of charge-traps in the lateral capacitors. B). The traps lead to a decrease in E_C and increase in P_r as artifacts in the PE loops.

Sc-Doping and Film Stress as Independent Tuning Parameters for E_C

Theoretical predictions and reports in literature have shown that the coercive field in ScAlN decreases as Sc-doping increases [6], [10]. However, we observe that the film deposition stress σ can provide an additional tuning knob for controlling the switching field that is decoupled from the extent of doping. Figure 5 shows a map of E_C and P_r comparing vertical capacitors on 200 nm 30% and 22% ScAlN (samples C and D respectively) deposited on identical 200 nm Pt BE. Even though sample D has a lower Sc-doping, it has a lower E_C and higher P_r over the entire range of capacitor sizes and frequencies tested. The films have very similar crystal quality as indicated by XRD-FWHM. The anomalous result can be attributed to the -83 MPa compressive stress in film C, which potentially degrades the ferroelectric properties, compared to film D which has favorable tensile stress of 102 MPa to realize a lower E_C and higher P_r.

CONCLUSIONS

Ferroelectric ScAlN thin film capacitors with 22% and 30% doping were tested over a wide range of frequencies and device sizes for two different thicknesses of 200 nm and 300 nm. The experimental results indicate that larger capacitors of 100 μm diameter operated at the lowest tested frequency of 1.5 kHz demonstrate the smallest E_C across all samples and substrates. A comparison of vertical and lateral capacitors shows that vertical capacitors reduce the impact of trapped charges seen in lateral capacitors, despite

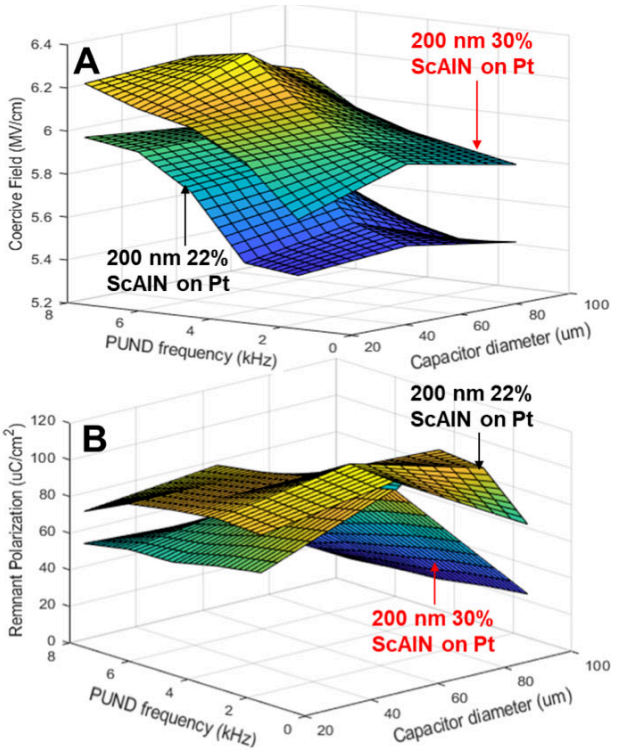

Figure 5: 3D map of A). E_C and B). P_r for 30% and 22% ScAlN (samples C and D) on Pt electrodes tested over the range of capacitor sizes (20-100 µm) and frequencies (1.5-7.5 kHz). In spite of lower Sc-doping, the 22% doped ScAlN has lower E_C and higher P_r due to a favorable tensile film stress of 102 MPa.

suffering from higher leakage due to a single AlN barrier film in the signal path. The observation of an anomalous lower E_C and higher P_r in 200 nm 22% ScAlN compared to its 30% doped counterpart presents the the opportunity to decouple the Sc-doping percentage and film stress towards engineering a more rapid reduction in coercive fields for ferroelectric ScAlN integration in the RF frontend.

ACKNOWLEDGEMENTS

This work was supported by the DARPA TUFEN program, and made use of the Cornell NanoScale Facility (NSF Grant NNCI-2025233) and the Cornell Center for Materials Research Shared Facilities which are supported through the NSF MRSEC program (DMR-1719875).

REFERENCES

[1] R. Ruby, P. Bradley, J. D. Larson, and Y. Oshmyansky, "PCS 1900 MHz duplexer using thin film bulk acoustic resonators (FBARs)," *Electron. Letters*, vol. 35, no. 10, pp. 794–795, May 1999.

[2] R. H. Olsson *et al*, "Post-CMOS compatible aluminum nitride MEMS filters and resonant sensors," *IEEE IFCS and Exposition*, 2007, pp. 412–419.

[3] M. Akiyama, K. Kano, and A. Teshigahara, "Influence of growth temperature and scandium concentration on piezoelectric response of scandium aluminum nitride alloy thin films," *Applied Physics Letters*, vol. 95, no. 16, p. 162107, Oct. 2009.

[4] P. Muralt, R. G. Polcawich, and S. Trolier-McKinstry, "Piezoelectric thin films for sensors, actuators, and energy harvesting," *MRS Bulletin*, vol. 34, no. 9, pp. 658–664, Jan. 2009.

[5] F. Tasnádi *et al*., "Origin of the anomalous piezoelectric response in wurtzite scxAl1-xN alloys," *Physical Review Letters*, vol. 104, no. 13, p. 137601, Apr. 2010.

[6] S. Fichtner, N. Wolff, F. Lofink, L. Kienle, and B. Wagner, "AlScN: A III-V semiconductor based ferroelectric," *Journal of Applied Physics*, vol. 125, no. 11, p. 114103, Mar. 2019.

[7] D. Wang *et al*., "Ferroelectric C-Axis Textured Aluminum Scandium Nitride Thin Films of 100 nm Thickness," *IEEE IFCS-ISAF*, Jul. 2020.

[8] J. Wang, M. Park, S. Mertin, T. Pensala, F. Ayazi, and A. Ansari, "A Film Bulk Acoustic Resonator Based on Ferroelectric Aluminum Scandium Nitride Films," *Journal of Microelectromechanical Systems*, vol. 29, no. 5, pp. 741–747, Oct. 2020.

[9] S. Rassay, F. Hakim, M. Ramezani, and R. Tabrizian, "Acoustically Coupled Wideband RF Filters with Bandwidth Reconfigurablity Using Ferroelectric Aluminum Scandium Nitride Film," in *Proceedings of the IEEE International Conference on Micro Electro Mechanical Systems (MEMS)*, pp. 1254–1257,2020.

[10] S. Yasuoka *et al*., "Effects of deposition conditions on the ferroelectric properties of (Al1- xSc x)N thin films," *Journal of Applied Physics*, vol. 128, no. 11, p. 114103, Sep. 2020.

[11] G. Giribaldi, M. Pirro, B. Herrera, M. Assylbekova, L. Colombo, and M. Rinaldi, "Compensation of Contact Nature-Dependent Asymmetry in the Leakage Current of Ferroelectric ScxAl1-xN Thin-Film Capacitors," in *Proceedings of the IEEE International Conference on Micro Electro Mechanical Systems (MEMS)*, 2021.

[12] V. Felmetsger, M. Mikhov, M. Ramezani, and R. Tabrizian, "Sputter Process Optimization for Al0.7Sc0.3N Piezoelectric Films," in *IEEE International Ultrasonics Symposium, IUS*, Oct. 2019, vol. 2019-October, pp. 2600–2603.

[13] B. Davaji, M. Abdelmajeed, A. Lal, T. Pennell, and V. Genova, "Sputtered AlN Lateral Bimorph: Process Integration Challenges and Opportunities," Jul. 2020.

[14] C. B. Sawyer, C. H. Tower, "Rochelle salt as a dielectric," *Physical Review*, vol. 35, no. 3, pp. 269–273, Feb. 1930.

[15] S. D. Traynor, T. D. Hadnagy, and L. Kammerdiner, "Capacitor test simulation of retention and imprint characteristics for ferroelectric memory operation," *Integr. Ferroelectr.*, vol. 16, no. 1–4, pp. 63–76, 1997.

[16] R. Meyer, R. Waser, K. Prume, T. Schmitz, and S. Tiedke, "Dynamic leakage current compensation in ferroelectric thin-film capacitor structures," *Applied Physics Letters*, vol. 86, no. 14, pp. 1–3, Apr. 2005.

[17] J. C. Tseng and J. G. Hwu, "Lateral nonuniformity effects of border traps on the characteristics of metal-oxide-semiconductor field-effect transistors subjected to high-field stresses," *IEEE Transactions on Electron Devices*, vol. 55, no. 6, pp. 1366–1372, Jun. 2008.

CONTACT

*Ved Gund – vvg3@cornell.edu